On-line Electrochemical Impedance Spectroscopy method for PV diagnosis system

Fadoua Borchani[1], *Souhir Sallem* [1], and *Mohamed Ben Ali Kammoun* [1]

[1] National School of Engineering Sfax, Tunisia

Abstract. PV fault conditions in photovoltaic (PV) systems reduce panel power performance and accelerate cell degradation. In this way, many research have recently turned to the diagnosis of PV generator to minimize the cost of the produced energy and ensure reliable power production. This paper proposes a new PV diagnosis system based on on-line Electrochemical Impedance Spectroscopy. This latter is used to estimate internal parameters of PV panel connected to a resistive load via a DC/DC boost converter. The Nyquist Diagram allows to plot and evaluate dynamic impedance response versus variable low frequency signal injected in conjunction with the high frequency system allowing to operate the PV in MPPT condition. The dynamic single diode model with a series resistance, a shunt resistance and a junction capacitance is used to design the PV model in MATLAB/Simulink. Simulations results are given for normal and for faulty operation whether in the PV panel or in the load. Referring to these results, it is concluded that the proposed diagnosis method allows to detect PV panel faults regardless of load variation.

1 Introduction

In the last decennary, PV systems have been largely integrated to product clean energy. Therefore, to ensure the continuity of energy production, a diagnosis of the PV system remains significant. In this way, a lot of research work have been focused on PV system diagnosis. For instance, in [1] the authors present types and causes of PV system failure and classify the electrical diagnostic methods into five methods which are methods based on statistical and signal processing approaches; I-V characteristics analysis; power losses analysis; voltage and current measurement and artificial intelligence techniques. [2-4] proposed a diagnosis method using a statistical method named Exponentially Weighted Moving Average (EWMA) chart to investigate faults namely short-circuit, open circuit and shading in PV system. The same method improved for multivariate (MEWMA) for fault detection and identification in DC side of PV system. In [5-7], the authors presented a fault diagnostic prototype employing the dynamic I-V characteristics as it has a remarkable shape in standard work condition and even in cases of fault diseases. In [8], the authors used both of power loss and I-V characteristics analysis to diagnose a PV system. In [9-11] a flexible fast fault localization method using the measured current, voltage and power was proposed. In [12], the authors develop an error detection method for PV systems using power losses analysis and a supervising system based on including the measured environmental conditions. According to these works, many methods for fault detection and diagnosis have been investigated in order to solve this issue. These techniques can be classified according to their efficiency, simplicity in terms of implementation, fast fault detection and diagnosis algorithms, adaptability for different PV technologies, fault classification, ability to identify multiple faults and ability to detect new faults.

In this paper, a diagnosis method based on Electrochemical Impedance Spectroscopy EIS is proposed [13]. This method is widely used in many fields such as faults detection in batteries and corrosion study. In PV system, this technique is used based on spectrometer to detect PV cell degradation or climatic influence in internal parameters. In this paper, a new use of this technique called 'online EIS' is proposed. It consists on 'on-line' detection and localisation of the PV system fault composed of a PV panel supplying a DC load via boost converter. The main work is resumed in this paper divided into four sections. The PV system modeling is presented in section 2. In section 3, the proposed diagnosis method is detailed, and results and discussion are given in section 4. The conclusion and future works will be provided in the last section of this paper.

2 PV system modeling

The. studied PV system in this paper is composed of a PV generator supplying a resistive load via a boost DC/DC convertert

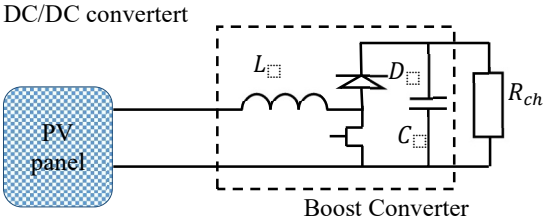

Fig. 1. studied PV system

2.1 PV cell modelling

In literature, a lot of research work have been focused on PV cell and PV panel modelling such as [14-15] which considered static PV model, and [16-17] which taken into consideration the effect of dynamic behaviour of the PV cell under sudden perturbations.

2.1.1 Static model

The one diode model and the two-diode model are the commonly used models in literature [14-15]. Many researchers have been concentrated on the one diode model three parameters [18] which characterize the ideal PV panel, the one diode model four parameters [19], which is more realistic since it includes the series resistance R_s. To present the semiconductor contact, the one diode model and five parameters is considered in [14,20] which describes the PV panel behaviour precisely. This model is composed of a current generator, one diode series resistances R_s and shunt resistance R_{sh} caused by various losses at the semiconductor level. The electric equivalent diagram of the PV panel is presented in figure 2.

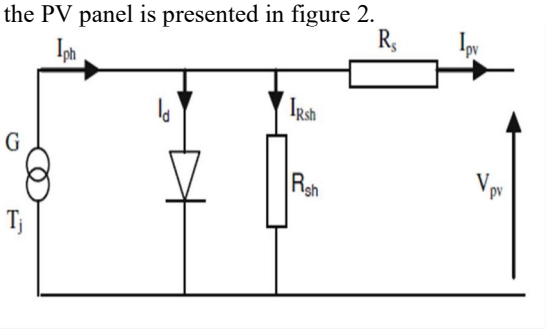

Fig. 2. One diode model

According to figure 2, the model can be expressed by the following nodal expression:

$$I_{pv} = I_{ph} - I_d - \frac{V_{pv}+I_{pv}R_s}{R_{sh}} \quad (1)$$

Where I_{pv} is the output current of the PV cell. V_{pv} is the output voltage of the PV cell. I_{ph} and I_d are expressed by the following equations

$$I_d = I_0\left(exp^{\frac{V_{pv}+I_{pv}R_s}{n V_t}} - 1\right) \quad (2)$$

$$I_0 = \frac{I_{sc_n}+K_i\Delta T}{Exp(\frac{V_{oc}+K_v\Delta T}{V_T})} \quad (3)$$

$$I_{ph} = (I_{sn} + K_i\Delta T)\frac{G}{G_n} \quad (4)$$

Where V_t is the thermal voltage, n is the diode ideality factor, I_{ph} is the short-circuit current at Standard Test Conditions, K_i is the current temperature coefficient of the PV panel, and G is the solar irradiance, V_{oc} is the open-circuit voltage at Standard Test Condition STC and K_v is the open-circuit voltage coefficient.

2.1.2 Dynamic model

Recently, a lot of study have been examined the dynamic attitude of the PV panel by adding a capacitance to the one diode model as present in the figure (3) [17]. The added capacitance describes the PN junction variation under various perturbations. According to [17], the added capacitance is the sum of three reactions of the PN junction: the Junction capacitance (C_j), the diffusion (C_d) and the breakdown capacitance (C_{bd}). In this paper, only (C_d) is considered since the PV cell is studied only

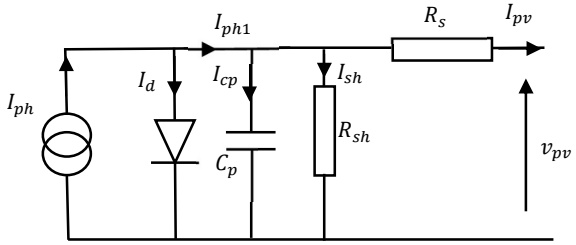

Fig. 3. Dynamic model

The (C_d) value is calculated using the following expression:

$$C_d = \frac{\tau I_d}{a V_T} \quad (5)$$

Where τ is the mean carrier lifetime.

In the rest of this paper, the Dynamic One Diode Model will be considered.

2.1.3 Internal parameters estimation

According to [21], the internal parameters of the PV cell namely series resistance, shunt resistance and junction capacitance are not constant, and their estimation is based on the electrical equivalent model or the measured $I-V$ curve. In [22-23] they assume respectively that the PV internal parameters depend on irradiance perturbation.as given at the bellow.

$$R_s = R_{s,stc} + \frac{V_t}{I_{sc}}\left(\frac{G}{G_n} \times \frac{T_{stc}}{T} - 1\right) \quad (6)$$

$$R_{sh} = R_{sh,stc}\left(\frac{G_n}{G}\right) \quad (7)$$

Based on the developed equations given below, the PV panel can be expressed as shown in figure 4. The model is implemented on Simulink allowing to obtain the current I_{ph1} (figure 3). The photovoltaic current is then deduced using a Simpower interface. This model helps better to describe both the static and the dynamic behavior of the PV cell under different operation zones

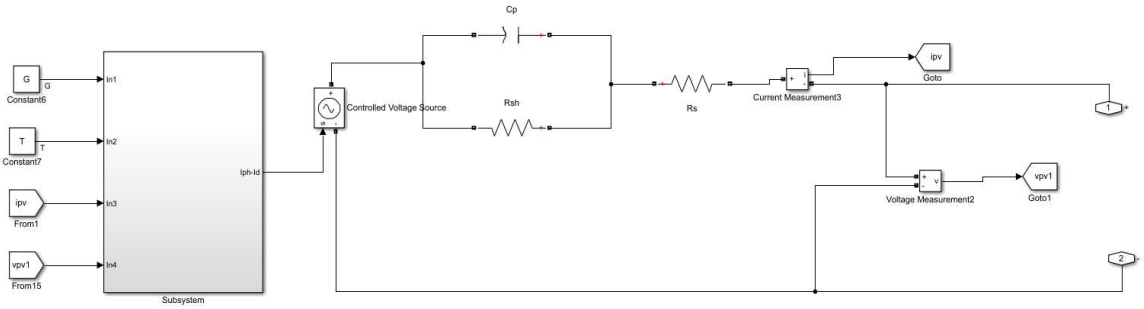

Fig. 4. The used PV panel model

2.2 Boost converter modelling

To extract the maximum power of the PV generator, a boost converter is used. This latter is described by Figure 5

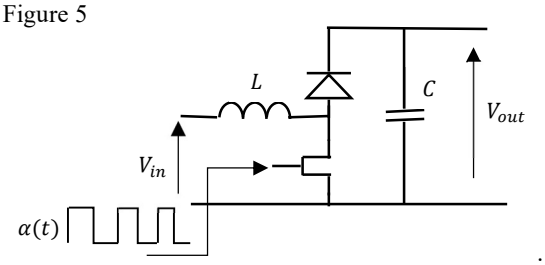

Fig. 5. Boost converter

The dynamic model of the boost converter is given by the equation (8) and equation (9).

$$\frac{di_L}{dt} = \frac{1}{L}(\alpha V_i + \bar{\alpha}\,\mathrm{sign}(i_L)(V_i - V_0)) \quad (8)$$

$$\frac{dV_0}{dt} = \frac{1}{C}(\bar{\alpha} i_L \mathrm{sign}(i_L) - i_0) \quad (9)$$

where V_o is the output voltage, α is the duty cycle and V_i is the input voltage. To calculate the boost converter parameters which are the capacitance value and the inductance value, the following expressions are used.

$$L = \frac{V_i}{\Delta I_{in} F}\alpha \quad (10)$$

$$C = \frac{I_{out}}{\Delta V_o F}\alpha \quad (11)$$

Where I_{in} and I_{out} are respectively the input and the output current. F is the commutation frequency of the DC/DC converter.

3 Proposed diagnosis method

The main objective of this work is to diagnose PV system under a sudden climatic perturbation or PV cells degradation under PV system operation [24-26].

The principle is to inject a variable low frequency signal in conjunction with the high-frequency pulse train applied to the gate driver of the DC/DC converter. The duty cycle α used to control the boost converter is then given by eq(12)

$$\alpha(t) = \alpha_{av} + a_d cos(\omega_0 t) \quad (12)$$

where α_{av} is the average duty cycle, a_d is the offset amplitude and ω_0 is the variable low-frequency injected in conjunction with α_{av}.

For each injected frequency ω_0, the PV voltage V_{pv} and the PV current I_{pv} are acquired and filtered to compute the real time dynamic PV impedance.

A Nyquist diagram $[\Re(Z_{PV}) \quad -\Im m(Z_{PV})]$ is then plotted allowing on one hand to estimate internal parameters of the PV panel namely series resistance, shunt resistance and junction capacitance and on the other hand to detect faults in the PV panel. Figure 6 plots the principle of dynamic PV impedance response.

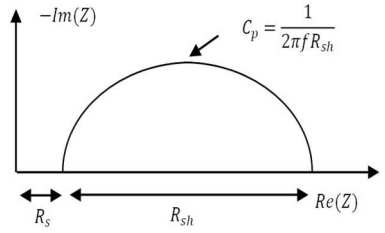

Fig. 6. The Nyquist diagram

The flowchart given in figure 7 explains the steps of the on-line PV impedance measurement using EIS technique

In fact, $V_{pv}(t)$ and $I_{pv}(t)$ are treated to eliminate the high frequency of the DC/DC converter F and to compute the corresponding mean values of these variables for every low frequency injected f. The values of $|V_{pv}|, \varphi_{Z_{pv}}, \Re(Z_{PV}), -\Im m(Z_{PV})$ are then stocked up until the maximum low frequency injected is reached.

4 Results and discussion

The process detailed in the previous flowchart is implemented to the studied PV system described by figure (1). The DC-DC converter is controlled via PWM signal with a constant duty cycle α_av at $F = 100kHz$. The small frequency signal $\omega_0\ (t)$ which frequency is varying between $50Hz$ and $90kHz$ is added to α_{av} as explained in Eq (12). Figure 8 shows the evolution of the injected signal to the gate driver of the DC/DC converter and Figure 9 plots the evolution of $i_{pv}(t)$ and $V_{pv}(t)$ versus time. These figures prove that the extra added signal doesn't affect the behavior of the PV panel since the duty is almost constant and its amplitude is very low compared to the PWM injected signal. Table 1 resumes the PV system parameters

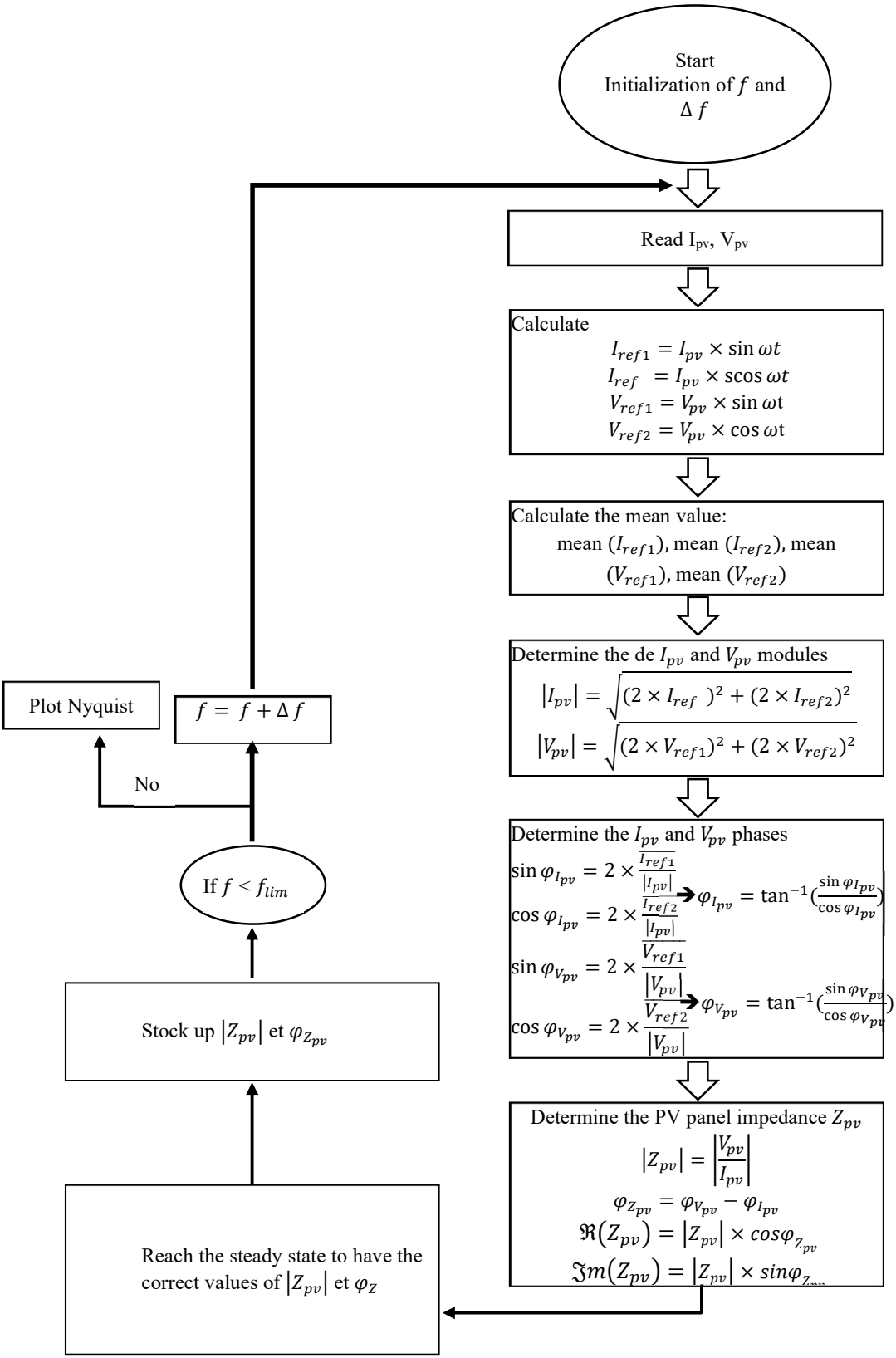

Fig. 7. Proposed technique to plot the Nyquist diagram in real work condition

Table 1. The PV system parameters.

PV panel parameters	
I_{sc}	3.8A
V_{oc}	21.1V
K_i	3e-3
K_v	-80e-3
G_n	1000 W/m^2
V_T	0.0257V
n	1
Boost converter parameters	
C	8.75e-3F
L	1.71e-1H

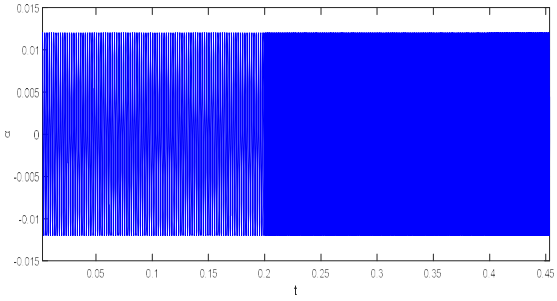

Fig. 8. The evolution of the gate driver injected signal versus time t(s)

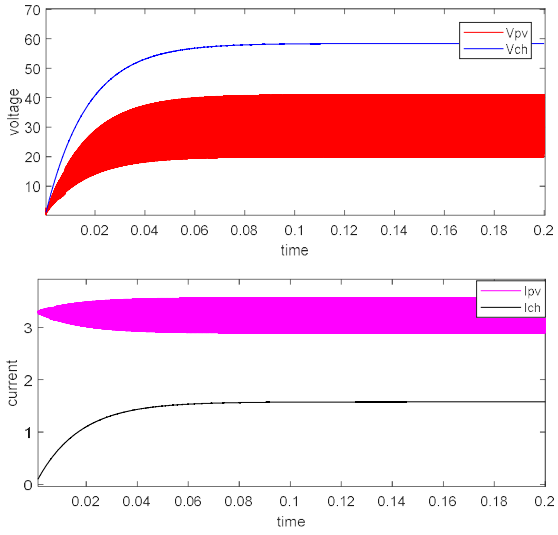

Fig. 9. Input and output voltage and currents of the DC/DC converter

To verify the reliability of the proposed process, the dynamic PV impedance is evaluated for five scenarios:

Scenario 1: the PV system is composed of two series PV panels exposed to constant irradiance $G_1 = 1000W/m^2$. The DC/DC converter allows to supply the resistance at the Maximum PV Power, $R_{Load} = 50\Omega$,

Scenario 2: the PV system is exposed uniformly to irradiance $G_2 = 400W/m^2$. for the same described operation in scenario 1, $R_{Load} = 50\Omega$,

Scenario 3: a shadow affects the first PV panel which is exposed to $G_2 = 400W/m^2$ instead of the second panel which is exposed to irradiance $G_1 = 1000W/m^2$. the irradiance is no longer uniform for the two panels, $R_{Load} = 50\Omega$,

Scenario 4: the two series PV panels are exposed to constant irradiance $G_1 = 1000W/m^2$ and the load was short circuited, $R_{Load} = 1\Omega$

Scenario 5: $R_{Load} = 1000\Omega$ to highlight the influence of the open circuit on the load level for the same PV cells.

Figure 10 plots the Nyquist Diagram for scenarios 1, 2 and 3. It is very clear that the impedance changes according to irradiance (Scenario 1 and Scenario 2). This confirms that the PV impedance depends on irradiance variation. In addition, in case of shading, the obtained dynamic PV impedance allows to detect the shading of the first PV panel since its response in Nyquist diagram is different from the expected impedance.

Figure 11 plots $|Z_{PV}|$ versus variable low frequency $f = \frac{\omega_0}{2\pi}$. This figure shows that the frequency response of the PV impedance is affected in case of shading especially for low frequency.

Consequently, this on-line PV impedance measurement is useful for internal parameters estimation in one hand, and for diagnose the PV system in the other hand

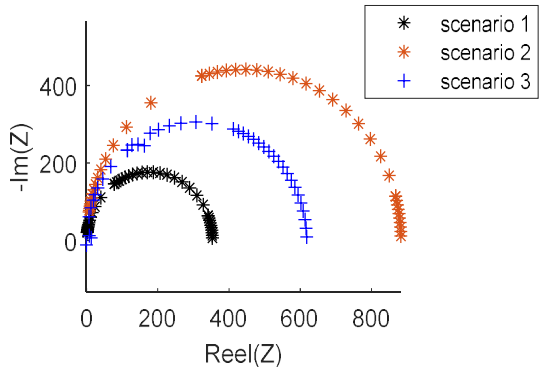

Fig. 10. Nyquist diagram$[\Re(Z_{PV}) \quad -\Im m(Z_{PV})]$ for the three scenarios.

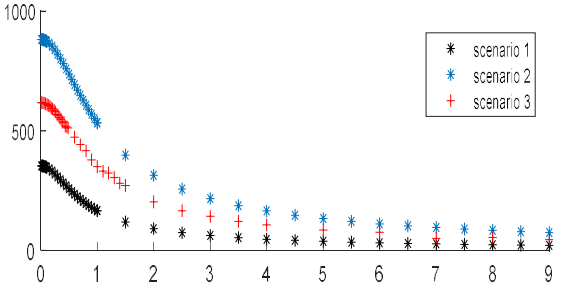

Fig. 11. $|Z_{PV}|$ versus f for the three scenarios.

According to scenarios 4 and 5, Figure 12 plots the PV voltage for three operation zones:

- Open circuit voltage zone,
- Mpp zone,
- Short circuit current zone

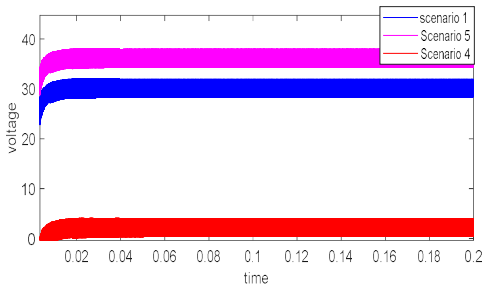

Fig. 12. PV current and voltage for scenario 1 scenario 4 and scenario 5

Figure 13 show the Nyquist diagram scenario 1 scenario 4 and scenario 5.

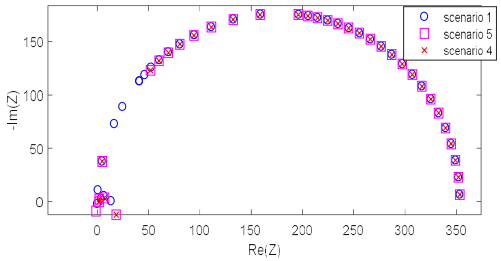

Fig. 13. Nyquist diagram $[\Re(Z_{PV}) \quad -\Im m(Z_{PV})]$ for scenario 1 scenario 4 and scenario 5

According to figure 12 and figure 13, the dynamic PV impedance remains constant for the three scenarios 1, 4 and 5 even the PV voltage depends on operation zone.

Consequently, this method allows to detect only faults in the PV cells independently of DC/DC converter or load faults

5 Conclusion

An on-line fault detection method for PV panels is presented in this paper. This method is based on 'on-line' Electrochemical Impedance Spectroscopy EIS. The PV system is composed of two series PV panels feeding a resistive load through a boost converter. The diagnosis method is based on photovoltaic voltage and current measurement and treatment through an implemented algorithm allowing to deduce the dynamic PV impedance for each injected frequency. Five scenarios are studied to evaluate the proposed method.

Simulation results prove that this method can detect and localise the faults such as shading in the PV panel separately from a load variation.

The frequency PV impedance response for various scenarios will be adopted to train a database for future work consisting to implement this method via an experimental setup.

References

1. A. Mellit, G.M. Tina, S.A. Kalogirou, Renew. Sust. Energ. Rev. **91**, 17 (2018)
2. Harrou F, Sun Y, Taghezouit B, Saidi A, Hamlati M-E, Renew Energy **116**, 15 (2018),
3. F. Harroua, B. Taghezouitb, Y Suna Energy Convers. and Manag. **180**, 13 (2019)
4. E Garoudja, F Harrou , Y Sun, K Kara, A Chouder, S. Silvestre Sol Energy **150**, 14 (2017)
5. S. Fadhela, C. Delphac, D. Diallob, I. Bahrib, A. Miganb, M. Trabelsid, M.F. Mimounid Sol Energy **179**, 10 (2019)
6. Z. Zhang, M. Ma, H. Wang, H. Wang, W. Ma, X. Zhang Sol Energy **225**, 15 (2021)
7. M. Maa, H.Liua, Z. Zhanga, P. Yunb, F. Liua Microelectron Reliab **100-101**, 6 (2017)
8. Y H Chen, R Liang, Y Tian,Wang IOP Conf. Ser: Earth Environ.Sci **40**, 15 (2016)
9. S. Zhou, M. Mao, L. Zhou, Y. Wan, X. Xi J-PV **10**, 8 (2020)
10. L. Chen X. Wang IEEE Trans Smart Grid **9**, 12 (2017)
11. S Dhar, R Patnaik,P Dash IEEE Trans Smart Grid **9**, 10 (2018)
12. A. Chouder S. Silvestre Energy Convers. Manag., **51**, 8 (2010)
13. M. A. Varnosfaderani, D. Strickland Vacuum **139**, 10 (2017)
14. I. Kashif, S. Zainal, T Hamed Sol Energy **95**, 9 (2011)
15. L Khemissi, B Khiar, R. Andoulsi, A. Cherif Sol Energy **86**, 13 (2012)
16. M. C. D. Piazza, M. Luna, G. Vitale J-PV **3**, 8 (2013)
17. K. A. Kim, C. Xu, L. Jin, P. T. Krein, J-PV **3**, 8 (2013)
18. P. Wolf, V. Benda Sol Energy **93**, 7 (2013)
19. G. Ciulla, V. L. Brano, V. D.Dio, G. Cipriani Renew. Sust. Energ. Rev. **32**, 13 (2014)
20. T. Ikegami, T. Maezono, F. Nakanishi, Y. Yamagata, K. Ebihara Sol. Energy Mater Sol. Cells **67**, 7 (2001)
21. R. Singha, M. Sharmab, R. Rawatc, C. Banerjeea Renew. Sust. Energ. Rev. **98**, 18 (2018)
22. J. D. Bastidas-Rodriguez, E. Franco, G. Petrone, Carlos, A. Ramos-Paja, G. Spagnuolo IEEE Trans. Ind. Electron. **62**, 10 (2015)
23. T. Ma, H. Yang, L. Lu Sol Energy **100**, 10 (2014)
24. D. A. Howey, P. D. Mitcheson, V. Yufit, G. J. Offer, N. P. Brandon, TVT **63**, 9 (2014)
25. R. Koch, R. Kuhn, I. Zilberman, A. Jossen, 16th Eur. Conf.P. E. A. **62**, 9 (2015)
26. O. I. Olayiwola, P. S. Barendse ECCE 8 (2017)